JOURNAL OF GEOPHYSICAL RESEARCH, VOL. 95, NO. D3, PAGES 2021-2034, FEBRUARY 28, 1990

Multifractals, Universality Classes and Satellite and Radar Measurements of Cloud and Rain Fields

SHAUN LOVEJOY AND DANIEL SCHERTZER

Department of Physics, McGill University, Montreal, Quebec, Canada

The extreme variability of cloud and rain fields poses serious problems in quantitative use of remotely sensed satellite and radar data. We show how to characterize this variability using scale invariant (sensor resolution independent) codimension functions which are exponents characterizing the probability distributions. These codimension functions in turn form a three parameter universality class. We review the properties of these multifractal measures and empirically evaluate the codimension functions as well as the universality classes for infrared and visible satellite cloud images using the new probability distribution/multiple scaling technique, refining previously published results and relating these to the established lognormal rain and cloud phenomenologies. We then show how to solve the radar observers' problem for multifractal radar reflectivity factors and to estimate the codimension function of rain from the radar. Finally, we reexamine some earlier (monofractal) analysis techniques in the light of our findings.

1. INTRODUCTION

The development of new in situ and remote measurement techniques has made large quantities of high-resolution geophysical data routinely available for analysis. In the case of satellite measurements of the atmosphere, their potential utility has lead to increasingly sophisticated algorithms for the estimation of geophysically significant parameters. One of the fields which has the longest history of remote measurements is rain and its associated cloud fields. These remote measurements have convincingly demonstrated not only the impressive ranges of spatial and temporal scales over which variability occurs, but also the extreme nature of fluctuations at fixed scales. This extreme variability is largely responsible for the difficulties in interpreting the data in terms of conventional physical parameters. For example, quantitative use of radar reflectivities typically makes repeated use of assumptions of subresolution homogeneity. First, in relating the measured "effective reflectivity factor" to the reflectivity factor and then in obtaining rain rates from the latter. A further uniformity assumption is usually made to adjust these rain estimates to rain gage values (here uniformity is needed to compare volume averaged radar quantities at one scale with time averaged gage network quantities at another). Quantitative estimates of cloud amount (or satellite rain estimation schemes) also implicitly use subsensor homogeneity assumptions in order to allow them to be calibrated with in situ data which typically involve averages at quite different time and space scales. The seriousness of problems caused by the variability is becoming more clearly understood: for example, a recent study by *Shih et al* [1988] showed that when identical algorithms were used to estimate cloud "fractions" over an identical "scene" viewed by two satellites differing in spatial resolution by a factor of 10, it was not uncommon for results to differ by factors of 2. In the radar estimation of rain, the extreme subsensor variability has contributed to ongoing debates about how best to calibrate the radar data from rain gages; debates that have been going on for nearly 40 years.

In a series of papers [*Lovejoy*, 1981, 1982; *Lovejoy and Schertzer*, 1983, 1985, 1986*a*, *b*; *Lovejoy and Mandelbrot*, 1985; *Schertzer and Lovejoy*, 1983, 1984, 1985a, b; 1986, 1987a,b; 1989, 1990*a*; *Lovejoy et al*, 1987] we have argued that we may expect geophysical fields generally, and atmospheric fields particularly, to exhibit scaling fractal structures over significant fractions of their dynamically important ranges. With the development of a series of new notions (particularly, multifractals and generalized scale invariance- see below), we now know that the types of scaling possible are very rich. This development of scaling ideas has spawned new data analysis techniques which have been important in investigating atmospheric fields. Furthermore, the theoretical difficulties encountered in dealing with the atmospheric observations have contributed to rapid advances in multifractals themselves.

The term "scaling" is used to indicate that certain aspects of a system (typically certain statistical exponents such as those found in energy spectra) are independent of scale. The related term "scale invariance" refers to systems in which the statistical properties of small and large scales are related by a scale changing operation involving only scale ratios: over the corresponding range, the system has no characteristic size. Scale invariant sets are generally fractals; fields and measures characterized by a single fractal dimension are here termed "mono-fractals" to distinguish them from multifractal measures which are characterized by an infinite hierarchy of dimensions. Although we do not wish to repeat these arguments in detail, the basic idea may be simply expressed. If we consider scaling as a symmetry principle (i.e., the system is unchanged under certain scale changing operations), then we may tentatively assume (a first approximation) that the symmetry is respected except for symmetry-breaking mechanisms.

More specifically, it has recently been shown [*Schertzer and Lovejoy*, 1987*a*, *b*] that multiplicative cascade processes precisely of the type that are believed to be responsible for the concentration of energy, water, and other fluxes into smaller and smaller regions of the atmosphere generically give rise to multifractal measures in which the increasingly intense regions are distributed over increasingly sparse fractal sets. Multifractal measures are much more relevant in geophysical applications than fractal sets, since geophysical quantities are best described as measures, with empirical data being functional approximations to the latter, (which as we shall see, are intrinsically strongly dependent on the resolution of the sensor). Multifractal

[1]Now at Etablissement d'Etudes et Recherche Météorologique/ Centre de Recherche en Météorologie Dynamique, Météorologie Nationale, Paris, France.

Paper number 89JD01653.
0148-0227/90/89JD-01653$05.00

measures are characterized by their scale invariant codimension function, which is an exponent function that determines how the probability distribution varies with scale. The geometry of sets and their associated fractal dimensions are secondary; the scale invariant dynamics (characterized by the generator of the measure) play the primary role.

We and others have already shown [*Lovejoy et al.*, 1987; *Gabriel et al.*, 1988] using an analysis technique called "functional box-counting" that both radar rain and satellite cloud fields are multifractal over various ranges in scale. In this paper, we first review some basic results on multifractals. We then give a more refined analysis of both fields using the new probability distribution/multiple scaling (PDMS) technique [*Lavallée et al.*, 1990], and show how to estimate the parameters of the (stochastic) generators of the fields. We then apply the method to geostationary satellite (GOES) data in both the visible and infrared wavelengths over the range 8-256 km. In section 4, we show theoretically how to solve the classical radar "observer's problem" in order to determine the codimension function for the radar reflectivity factor from the corresponding codimension function of the measured effective radar reflectivity factor. Standard assumptions (which relate the rain field to the reflectivity factor by a power law) then imply that the rain field codimension function is obtained by a simple linear transformation of the orders of singularities. Finally, in two fairly technical appendices, we discuss several data analysis techniques that were primarily designed to study monodimensional fractal sets. We then argue that many apparently contradictory results (including reports of scale breaking) reported in the literature can be understood if these fields are multifractal.

2. MULTIFRACTAL MEASURES

2.1. Discussion

Based on studies of certain fractal sets obtained either as purely geometric constructs, or associated with certain stochastic processes, *Mandelbrot* [1982] used these sets as models of the geometry of various natural systems. However, few natural systems are sets (they are usually best treated as fields or measures), and it soon became clear [*Hentschel and Proccacia*, 1983; *Grassberger*, 1983; *Schertzer and Lovejoy*, 1983; *Benzi et al*, 1984, *Frisch and Parisi*, 1985], that such measures are fundamentally characterized not by a single dimension, but by a dimension function (sometimes called the "spectrum of singularities"). Furthermore, this dimension function is simply related to the probability distribution. In fractal sets, the concept of fractal dimension is important because it is invariant under transformations of scale. In fractal measures, the notions of scaling (or scale invariance) and the generator of the measure are more basic.

Geophysical systems typically have variability extending down to very small scales η (often 1 mm or less) and are therefore usually observed (literally "measured") at scales (L) with scale ratio $\lambda = L/\eta >> 1$. It is therefore natural to consider the underlying phenomenon as a fractal measure, and the empirically accessible measurements (e.g., satellite photos) as a series of associated functions (denoted $f_\lambda(\mathbf{r})$), whose properties will depend greatly on the averaging scale ratio λ (e.g. on the size of a pixel). Qualitatively, the relationship of a series of lower and lower resolutions (i.e. f_λ as $\lambda \to \infty$) to the underlying multifractal measure is that as the resolution decreases, the structures are more and more smoothed out, are found to occupy an increasing fraction of the image, while simultaneously decreasing in value (e.g., dimming) to compensate. Since over our range of interest, there is no characteristic scale, this behavior is algebraic and can be expressed as follows (algebraic relations are for the moment valid to within proportionality constants and log corrections; see below)

$$\Pr(f_\lambda > \lambda^\gamma) \approx \lambda^{-c(\gamma)} \quad (1)$$

where Pr means probability, γ is the order of singularity associated with the pixel value f_λ, and $c(\gamma)$ is the associated codimension (the dimension of the underlying space (d) minus the corresponding dimension d(γ)). Equation (1) is the general characterization of multifractal fields and arises directly as the result of multiplicative cascade processes [*Schertzer and Lovejoy*, 1987a, b]. This equation shows that $c(\gamma)$ is directly related to the probability distribution. Note that in (1) and below, we ignore any logarithmic corrections. This fact will be used below as the basis for empirically estimating $c(\gamma)$. Qualitatively, γ is the resolution-independent characterization of the intensity of the feature with brightness f_λ, whereas, $c(\gamma)$ is the resolution independent characterization of the image fraction occupied by features with brightness f_λ.

For those who are familiar with multifractals, it is worth noting here that we have denoted the orders of singularities by the symbol γ because the atmospheric quantities of interest are modelled by densities of multifractal measures (such as f) and γ gives the orders of these singularities directly. In other systems such as phase space portraits of strange attractors (e.g. *Halsey et al* 1986), it is more usual to treat the singularities of the measures (rather than their densities) usually denoted by the symbol α; the relation between α and γ being $\gamma = d - \alpha$ where d is the dimension of space in which the process occurs. Furthermore, we use the codimension function $c(\gamma)$ rather than a dimension function since we are really interested in a family of measures each identical except for the dimension of the space in which it is embedded (in some applications it is even useful to take the latter as a fractal set, e.g. the global meterological measuring network), and the codimensions specify the probabilities independently of the latter. In contrast, in studying strange attractors, d is usually kept fixed and the dimension is denoted $f(\alpha)$. We therefore have $f(\alpha) = d - c(d-\alpha)$.

We can now appreciate some of the difficulties encountered in many of the early studies, where multifractal phenomena were analyzed with methods originally designed for studying sets (e.g., area-perimeter relations, distribution of areas, dimensions of graphs, box counting: see appendices A and B). Even before the analysis begins, experimental measuring devices integrate the underlying measure over a scale L, converting it into a (spatially or temporally discretized) function. This function is then converted into a set with the same resolution, typically with the help of thresholds. Finally the geometric properties of the resulting set are characterized by (at most) a few exponents (e.g., dimensions, area-perimeter exponents) essentially by degrading the resolution of these sets. Although careful and systematic study of the properties of the sets as functions of scale and threshold (such as with "functional box counting" - [*Lovejoy et al.*, 1987; *Gabriel et al.*, 1988] can be used to estimate $c(\gamma)$, such methods are indirect and are less satisfactory than other methods such as trace moments [*Schertzer and Lovejoy*, 1987*a*] or the PDMS method [*Lavallée et al.*, 1990]. For comparison, functional box-counting exploits (1) by transforming the function f_λ into an exceedance set (see Appendix A) and covering the latter with larger and larger boxes. The fraction of the scene covered by boxes of scale λ is the probability in (1). The method works by degrading the resolution of the exceedance sets, rather than of the measures themselves. The approach described below is more straightforward and statistically robust, since it is defined directly by the measures f_λ rather than via associated sets. In contrast, the use of what might be termed

"monofractal" analysis techniques (i.e., techniques designed primarily for analyzing sets) can easily lead to seemingly contradictory results, and even to spurious breaks in the scaling (see appendices).

2.2. *Some Properties of Multifractal Measures*

The extreme variability (intermittency) of the atmosphere results from the concentration of various conserved fluxes (energy, concentration variance, etc.) into smaller and smaller regions by the action of nonlinear interactions and instabilities operating over wide ranges in scale. Even when the exact dynamical equations (and corresponding conserved quantities) are not known, it is still likely that such cascades are responsible for much of the observed variability. Fairly recently, research in turbulence has shown that cascades of this sort where the large scale multiplicatively modulates the small, when carried out over wide enough ranges of scale with a repeating (scale invariant) mechanism, generally leads to multifractal measures [*Schertzer and Lovejoy*, 1987*a*, *b*]. Such measures can be regarded as superpositions of singularities (order γ) each distributed over sets with fractal dimension $d(\gamma)$: see (1). In what follows, we provide a brief summary of some of the properties of these measures.

Formula (1) has an equivalent statement in terms of the statistical moments of f_λ:

$$\langle f_\lambda^h \rangle = \lambda^{K(h)} = \int \lambda^{h\gamma} d\Pr \approx \int \lambda^{h\gamma - c(\gamma)} d\gamma \qquad (2)$$

where angle brackets indicate ensemble (statistical) averaging (note that here, and most of this paper, we systematically ignore log corrections to the scaling laws as well as scale independent constants such as c'(γ) on the right hand side of (2)). Hence, using the method of steepest descents, we obtain

$$K(h) = \max_\gamma (h\gamma - c(\gamma)) \qquad (3)$$

This (Legendre) transformation arises because in the limit $\lambda \to \infty$, for each moment h, there is a corresponding singularity γ_h which dominates the average: $h = c'(\gamma_h)$. The Legendre transformation is easy to obtain graphically: it is simply the maximum distance between the line $h\gamma$ and the curve $c(\gamma)$. Note that because the Legendre transform is equal to its inverse, we also obtain

$$c(\gamma) = \max_h (h\gamma - K(h)) \qquad (4)$$

showing the complete equivalence between a description in terms of moments $K(h)$ or probabilities $c(\gamma)$. It is also possible to define another codimension function associated with moments of various orders:

$$C(h) = \frac{K(h)}{h - 1} \qquad (5)$$

A great simplification in multifractal analysis and modeling occurs because for quantities conserved by the cascade, the $c(\gamma)$ function is characterized by the following two parameter functional forms or "universality classes" (*Schertzer and Lovejoy*, [1987*a*, *b*])

$$c(\gamma) = C_1 \left(\frac{\gamma}{C_1 \alpha'} + \frac{1}{\alpha} \right)^{\alpha'} \qquad (6)$$

with $0 \le C_1 \le d$, $0 \le \alpha \le 2$, $1/\alpha + 1/\alpha' = 1$. When $\alpha=1$, we obtain $c(\gamma)=C_1 \exp(\gamma/C_1 - 1)$. The corresponding universal $K(h)$ function is given by

$$K(h) = \frac{C_1 \alpha'}{\alpha} (h^\alpha - h) \qquad (7)$$

(again, for $\alpha=1$, we have $K(h)=C_1 h \log h$). When $\alpha<2$, (7) only holds for $h \ge 0$; for $h<0$, $K(h)=\infty$. The above functions are for conserved (stationary) quantities and are the multiplicative analogs of the standard central limit theorem for the addition of random variables, the case $\alpha = 2$ corresponding to (log) Gaussian processes, and $\alpha < 2$ to (log) Levy processes. Closer analysis shows that there are actually 5 qualitatively different cases; $\alpha=2$, $1< \alpha <2$, $\alpha=1$, $0< \alpha <1$, $\alpha=0$ corresponding to log normal multifractals, multifractals with unbounded singularities, log Cauchy multifractals, multifractals with bounded singularities (α' is negative), and the monofractal "β model" respectively (*Schertzer et al* [1988, 1989]). Furthermore, as discussed elsewhere (especially *Schertzer and Lovejoy* [1987a]), the terms lognormal, log Levy are not fully correct, it would be better to say multifractals with gaussian or Levy generators. The universality arises from the fact that the only stable and attractive generators are gaussian or Levy "1/f noises" (*Schertzer and Lovejoy* [1987a,b]).

The only caveate required is that since $\lambda^{K(h)} = \langle f_\lambda^h \rangle = \langle \exp(h \log f_\lambda) \rangle$ is the Laplace transform of the generator $\log f_\lambda$, only those Levy variables which possess Laplace transforms are admissible generators; these are the so-called extremal (maximally asymmetric) Levy variables. For $0<\alpha<1$ these extremal Levys are classical (e.g. *Feller* [1971]; see *Fan* [1989a, b] for an exact mathematical treatment of the corresponding noise). However, for $1<\alpha<2$, the extremal Levys are far from being classical; for this range of α, Fourier techniques are usually used. In *Schertzer and Lovejoy* [1990a] (appendix A), we proposed a unified Laplace treatment for all the Levy extremals for $0<\alpha\le 2$. *Schertzer and Lovejoy* [1990a] present graphs showing these families of curves.

For other quantities, related to the conserved quantities by either dimensional and/or power law relations, the corresponding $c(\gamma)$ functions can be obtained by the linear transformation $\gamma \to a\gamma + b$. For example, in turbulent cascades, the energy flux ε is conserved, and fluctuations in components of the velocity field are obtained by $\Delta v = \varepsilon^{1/3} \lambda^{-1/3}$; hence $a = -b = 1/3$. For passive scalar clouds (see *Schertzer and Lovejoy* [1987*a*, *b*] and *Wilson et al.* [1990] for details on these multifractal cloud and rain models), the corresponding quantities are $\Delta\rho = \varphi^{1/3} \lambda^{-1/3}$, where $\varphi = \chi^{3/2} \varepsilon^{-1/2}$ and χ is the variance flux of the passive scalar concentration ρ. Similarly, semi-empirical radar estimates of rain rate (R) from radar reflectivity factors (Z) use relationships of the form $Z \propto R^B$ with B a calibration constant (usually, $B \approx 1.6$). Allowing for these linear transformations of γ, we obtain the following three parameter universality classes for nonconserved quantities:

$$c(\gamma) = c_0 \left(1 - \frac{\gamma}{\gamma_0} \right)^{\alpha'} \qquad (8)$$

with

$$c_0 = C_1 \left(\frac{-b}{C_1 \alpha'} + \frac{1}{\alpha} \right)^{\alpha'} \qquad (9a)$$

$$\gamma_0 = -\frac{a C_1 \alpha'}{\alpha} + b \qquad (9b)$$

Since two of the parameters c_0, γ_0 depend on three fundamental

parameters a, b, C_1, we will not be able to unambiguously determine the latter from the former. Additional information (supplied perhaps by theoretical considerations) such as the relationship of the field to that of the conserved fluxes is required.

In empirical parameterizations of $c(\gamma)$, it is convenient to introduce yet another equivalent parameterization based on the parameters C_t, γ_t:

$$c(\gamma) = C_t\left(\frac{\gamma+\gamma_t}{C_t\alpha'} + \frac{1}{\alpha}\right)^{\alpha'} \tag{10}$$

Which under Legendre transformation, gives

$$K(h) = \frac{C_t\alpha'}{\alpha}(h^{\alpha}-h) - h\gamma_t \tag{11}$$

The above is useful in graphical parameter estimates, since it enables one to conveniently exploit a special property of the two parameter universality classes (equation (5)). As pointed out by *Schertzer and Lovejoy* [1990*a*], these classes have the special point satisfying $c(C_1)=C_1$, $c'(C_1)=1$ independent of α. With the above parameterization (the subscript t indicates tangent), we obtain the analogous property (used in section 3) for the three parameter classes:

$$\begin{aligned} c(C_t - \gamma_t) &= C_t \\ c'(C_t - \gamma_t) &= 1 \end{aligned} \tag{12}$$

Before discussing the analysis of satellite and radar data using the above formalism, we must first discuss a complication which arises because of a basic distinction between "bare" and "dressed" cascade quantities. The bare quantities are essentially theoretical: they are obtained after a cascade process has proceeded only over a finite range of scales; strictly speaking, (10), and (11) apply only to these quantities. The experimentally accessible quantities are different; they are obtained by integrating cascades (with a measuring device) over scales much larger than the inner scale of the cascade (which in the atmosphere is typically of the order of 1 mm). The properties of such spatial (and/or) temporal averages are approximated by those of the dressed cascades, i.e., those in which the cascade has proceeded down to the small-scale limit and then integrated over a finite scale. The small-scale limit of these multiplicative processes is mathematically singular and is responsible for this basic distinction.

Unlike the bare cascade, the dressed cascade displays the interesting phenomenon of divergence of high-order statistical moments, that is

$$\langle \varepsilon^h \rangle \to \infty \quad h \geq h_d \tag{13}$$

Where h_d is the critical exponent for divergence. In this sense, the dressed quantities are more variable than the bare quantities (whose positive moments are all finite). The precise condition for divergence is quite simple [*Schertzer and Lovejoy*, 1987*a*, *b*]:

$$C(h_d)=d(A) \tag{14}$$

where A is the averaging set (e.g., line, plane, or fractal in the case of typical measuring networks) over which the process is averaged. The phenomenon of divergence of high-order statistical moments arises directly from the fact that $C(h)$ is generally unbounded, and hence for any averaging set A, for large enough h, $C(h)>d(A)$. In the universality classes above, the only exception occurs when $\alpha<1$, which yields $\max(C(h)) = C_t/(1-\alpha) - \gamma_t$ and the latter can be $\leq d(A)$ (*Schertzer and Lovejoy* [1983 1985*a*, *b*] discuss a discrete rather than continuous cascade model outside the above universality classes called the "α" model, in which this also occurs). Note that even in the latter case, divergence will still occur if the set A is sufficiently sparse that $d(A)$ is small enough.

Rewriting the above, we obtain the following equation for h_d:

$$K(h_d)=d(A)(h_d-1) \tag{15}$$

$$\frac{C_t\alpha'}{\alpha}h_d^{\alpha} + h_d\left(-\gamma_t - d(A) - \frac{C_t\alpha'}{\alpha}\right) + d(A)=0$$

Corresponding to h_d, there is a critical singularity γ_d such that $\gamma_d=K(h_d)$. The functional forms for the three-parameter universality classes are therefore valid for the observable (dressed) quantities only for $h\leq h_d$, $\gamma\leq\gamma_d$ with γ_d written explicitly as

$$\gamma_d = C_t\alpha'\left(h_d^{\alpha-1} - \frac{1}{\alpha}\right) - \gamma_t \tag{16}$$

For $\gamma>\gamma_d$, $c(\gamma)$ is a straight line with slope h_d. For $h>h_d$, the moments $\langle \varepsilon^h \rangle \to \infty$; hence, strictly speaking, $K(h)$ is no longer defined. However, experimentally, finite sample sizes are used to estimate (infinite) ensemble averages, and we obtain the interesting phenomenon of pseudo-scaling [see *Schertzer and Lovejoy*, 1987*a*, *b*; *Lavallée et al.*, 1990]. Like α, estimating γ_d from the data is difficult because it too is sensitive to the low-probability, large γ, $c(\gamma)$ part of the function. It is therefore of interest to develop approximate graphical methods for its estimation (see below; Seed et al., manuscript in preparation 1990).

We have already discussed the fact that the various (bare) universality classes are lognormal ($\alpha=2$) and log-levy ($\alpha<2$), respectively. When α is not much smaller than 2, the latter are in turn approximately lognormal, since, with the exception of their extreme tails, these Levy distributions are themselves nearly normal (this "tail" is pushed to lower and lower probability levels as $\alpha\to 2$). Our findings here are therefore consistent with the widespread hydrological, meteorological (and generally geophysical) lognormal phenomenology. Of particular relevance here are numerous studies that have claimed that rain rates, cloud and radar echo sizes, heights and lifetimes, as well as total rain output from storms over their lifetimes are either lognormal or "truncated lognormal" distributions [*Lopez*, 1977*a*; *Drufuca*, 1977; *Houze and Cheng*, 1977; *Konrad*, 1978, *Warner and Austin*, 1978; etc.]. Furthermore, the cascade models that generate them are actually just concrete implementations of vague laws of "proportional effects" (see, e.g: *Lopez* [1977b] for an invocation of this law in the rain context).

The above comments need only minor modification when dealing with dressed quantities, since compared with the bare quantities, the former have even stronger (algebraic) extreme fluctuations, but are virtually the same for nonextreme fluctuations. *Waymire* [1985], *Waymire and Gupta* [1990] have used the expression "fat-tailed" for such (asymptotically algebraic) distributions, and "long-tailed" for the lognomal law (it could equally well be applied to the log-Levy cases), to distinguish these distributions from standard exponential "thin-tailed" distributions. Several years ago [*Schertzer and Lovejoy*, 1985*a*, *b*], we used the expression "hyperbolic intermittency" to describe the effect of this strong variability. It has been empirically estimated in a variety of meteorological fields: $h_d\approx 5$, for temperature [*Lovejoy and Schertzer*, 1986*a*, *b*, *Ladoy et al.*, 1986], $h_d\approx 1.66$ in changes in storm-integrated rain rate [*Lovejoy*, 1981], $h_d\approx 1.06$ in radar reflectivity factors of rain [*Schertzer and Lovejoy*, 1987*a*, *b*], and respectively. $h_d\approx 5$ and

3.33 for wind speed and potential temperatures [*Schertzer and Lovejoy*, 1985*a*, *b*]. The recent study by A. Seed et al., (manuscript preparation, 1990) has provided more insight into the problem by showing that although the parameters defining $c(\gamma)$ may not change much from one meteorological situation to another, h_d could vary considerably, since they find empirically $0.3<\alpha<0.6$ and from (15), we find that when $\alpha<1$, its value is particularly sensitive to small changes in the parameters C_t, γ_t, α. This is perhaps not surprising since h_d and the other parameters metnioned above are statistical and very large sample sizes will be needed to provide good estimates of the ensemble average values.

3. ESTIMATING c(γ) FOR SATELLITE CLOUD RADIANCES

3.1. PDMS technique

We seek to directly apply (1) to determining the scale invariant codimension function $c(\gamma)$. To do this, we must first fully nondimensionalize (1); we have already introduced the dimensionless scale ratio λ to nondimensionalize the scales, we must also nondimensionalize f this is conveniently done by using the large-scale average f_{λ_I} as a reference value for the measure where λ_I denotes the scale ratio corresponding to the large (I for image scale; $\lambda_I=L_I/\eta$). Using an overbar to denote the values of the function normalized in this way, we write: $\bar{f_\lambda} = f_\lambda/f_{\lambda_I}$. Theoretically, the latter should really be the ensemble (i.e., climatological) average of the random process at scale λ_I; the sample average being an approximation to the latter. We therefore obtain

$$\Pr\left(\bar{f_\lambda} > \lambda^\gamma\right) = F\,\lambda^{-c(\gamma)} \quad (\lambda \geq 1) \qquad (17)$$

where F is a prefactor which is only a function of γ and $\log\lambda$ (for example, if F contains a $(\log\lambda)^\delta$ dependency, δ is called a "sub-codimenison"). Taking logs and rearranging, we obtain

$$c(\gamma) = -\frac{\log \Pr\left((\log \bar{f_\lambda})/(\log\lambda) > \gamma\right)}{\log\lambda} - \frac{\log F}{\log\lambda} \qquad (18)$$

Hence, plotting the normalized log probability distribution ($-\log\Pr/\log\lambda$) against the normalized log intensity ($\log \bar{f_\lambda}/\log\lambda$) we obtain the resolution (λ) independent function $c(\gamma)$. To empirically test this multiple scaling behavior, we therefore take our empirical field and successively degrade it by averaging, obtaining a series of functions $f_{\lambda_1}(\mathbf{r})$, $f_{\lambda_2}(\mathbf{r})$, $f_{\lambda_n}(\mathbf{r})$, which simulates the results of sensors with successively lower resolutions with $\lambda_I=L_I/\eta>\lambda_n\geq\lambda_s>>1$, with λ_s the ratio of sensor scale to the inner scale of the variability. Successive factors of 2 can be easily implemented recursively. Note that we must not nonlinearly transform our radiance field (e.g., by transforming from radiances to equivalent blackbody temperatures), since this does not simulate the result of a lower resolution sensor. Furthermore, the normalization based on λ_I implicitly assumes that the probability distribution in (17) is either from a single scene or from several independent scenes. If single scenes are used, then we cannot obtain information on the codimension for values of $c>d(A)$, since the corresponding structures would have negative dimensions. However, when many realizations are available, the effective dimension of the sample can be larger, and higher values of $c(\gamma)$ can be determined; see *Lavallée et al.*, [1990] for discussion of this "sampling dimension." Finally, if many dependent samples are used (as in the use of time series of images in A. Seed et al.,(manuscript in preparation, 1990), then an "effective" λ_I can be determined from regression (as can $\bar{f}_{\lambda_I}$).

The Probability Distribution/Multiple Scaling (PDMS) technique refers to the direct exploitation of (17,18) to obtain $c(\gamma)$. This direct method has a number of advantages when compared to the conventional route (via the moments K(h) followed by Legendre transformation; see for example *Halsey et al.* [1986]) not the least of which is that it avoids the problem of estimating high order moments which may in fact diverge (see (13)). The PDMS method can be implemented in various ways. In *Lavallée et al.* [1990], histograms of all the values of $\bar{f_\lambda} = f_\lambda/f_{\lambda_I}$ at the various resolutions λ were produced, taking for the value of $\bar{f}_{\lambda_I}$ the mean of all the sample spatial averages at scale λ_I (the number of "scenes"/ satellite pictures, etc.). From the histogram, the largest to smallest values were summed to yield the probability distribution. Finally, $c(\gamma)$ was determined as the absolute slope of plots of $\log\Pr$ against $\log\lambda$ for given values of γ. This method has the advantage of readily taking into account the slowly varying prefactor F, since $\log F$ is simply the intercept at $\log\lambda=0$. See *Lavallée et al.* [1990] for a much more complete discussion of this method including theoretical considerations and numerical simulations.

In this paper, we used a slightly different method inspired by "functional box-counting" (*Lovejoy et al.* [1987]), in which the probability distributions at various scales λ was determined differently. The data at highest resolution (λ_S) was covered with a series of lower resolution grids (the "boxes") as explained above. However, rather than using the average value over each box (and create histograms of these averages), we used the maximum value in each $\lambda X\lambda$ box (denoted $\max_\lambda(\bar{f}_{\lambda_S})$). Since the function was not averaged, the singularity corresponding to each maximum value was simply estimated as $\gamma = (\log\max_\lambda(\bar{f}_{\lambda_S}))/\log\lambda_S$. The corresponding $c(\gamma)$ for each resolution λ was then estimated as $-\log\Pr/\log\lambda$ (we assumed $\log\lambda>>\log F$, ignoring the prefactor in (17)). Finally, we took the average $c(\gamma)$ function over a series of resolutions λ, indicating the scatter with one standard deviation error bars.

Figures 1*a*, 1*b* show the results when this technique is applied to five visible and five infrared GOES pictures over Montreal,

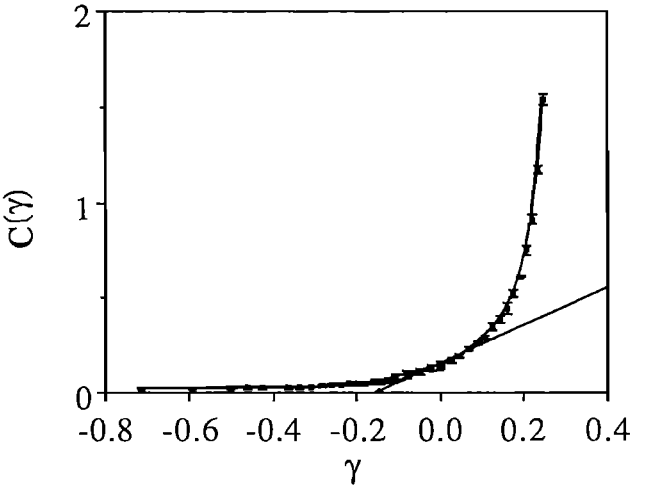

Fig. 1a. PDMS estimates of the function $c(\gamma)$ from the five visible GOES images over 1024 X 1024 km at 8 km resolution discussed in the text. The points indicate the mean $c(\gamma)$ curve obtained by averaging the six individual $c(\gamma)$ functions obtained at 8, 16, 32, 64, 128, 256 km scales (the histograms associated with 512 and 1,024 km did not have enough points and were not used). The error bars indicate one standard deviation (and were of average magnitude ±0.011), showing that the $c(\gamma)$ function was nearly scale invariant over this range. The solid line is the least mean squares fit to the universal form (equation (8)) (α'= -1.70, α = 0.63). The standard error of the fit was ±0.011. The straight line is the line slope 1, which is tangent to the curve. The value of $c(\gamma)$ where this occurs is C_t, and the point where the line intersects the γ axis is $-\gamma_t$.

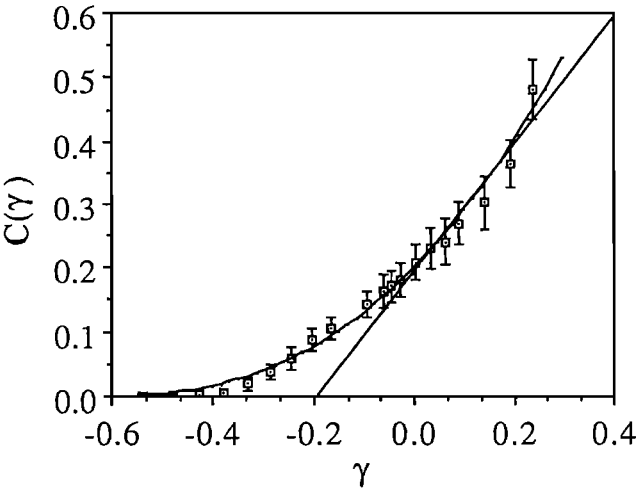

Fig. 1b. PDMS estimates of the function $c(\gamma)$ from the five infrared GOES images discussed in the text with the same range of scales and format as Figure 1*a*. The mean standard error was ±0.023, and the best fit regression to (8) yielded α'=2.52, α=1.66. The standard error of the fit was ±0.015.

respectively. The original (raw) satellite pictures were first resampled on a regular 8 x 8 km grid over a region of 1024 x 1024 km. As can be seen, all the distributions are nearly coincident, in accord with the multifractal nature of the fields. To judge the closeness of the fits, we calculated the mean $c(\gamma)$ curves as well as the standard deviations for 8, 16, 32, 64, 128, and 256 km, finding that the variation is small, being typically about ±0.02 in (γ), which is more accurate than estimates obtained using functional box counting on similar data (*Gabriel et al.*, [1988] found accuracies of about ±0.05).

3.2. *Parameter Estimation, and Universality classes of* $c(\gamma)$

We have already argued that the resolution independent codimension function $c(\gamma)$ is of considerably more interest than particular values of the function and that the latter is determined by γ_t, α, and C_t. The difficulty in testing these ideas empirically is that the key parameter α' (recall $1/\alpha'+1/\alpha=1$) characterizes the concavity of $c(\gamma)$, which is pronounced only when γ and $c(\gamma)$ vary over a substantial range. From the point of view of nonlinear regression, to fit γ_t, C_t, α' to the data, we find that C_t and α' are highly correlated, and hence parameter estimates are not very sharp. *Gabriel et al.*, [1988] used functional box counting, yielding less accurate estimates of $c(\gamma)$ than those obtained here. The issue was avoided by assuming α'=2 and testing the consistency of the data with that hypothesis.

Here we outline a simple graphical method which proves quite accurate. The easiest parameter to estimate graphically is $c_0=c(0)$, which yields c_0=0.16, 0.20 for visible and IR curves, respectively. However, C_t, γ_t can also be found quite easily. From (10), we recall that $c(\gamma)$ has the property that $c(C_t-\gamma_t)=C_t$ and $c'(C_t-\gamma_t)=1$ independent of α. This implies that a line slope 1 will be tangent to $c(\gamma)$ at the point $c(\gamma)=C_t$ and will intersect the γ axis at the point $\gamma=-\gamma_t$. Figures 1*a* and 1*b* show the construction lines, which yield C_t=0.21, 0.29, and γ_t=0.15, 0.19 for the visible and IR curves, respectively. Note that all three parameters estimated this way depend on the values of the curve $c(\gamma)$ in the statistically well-defined region near γ=0, rather than on the large γ regime corresponding to extremely low probabilities, or the small negative γ regime which could easily be contaminated by noise. Using (9*a*) and (9*b*) we can obtain the estimates $\alpha \approx 0.65$, 1.7 for visible and IR, respectively.

To improve on these results requires complex (nonlinear) regression. Here we determined α' by a least squares regression on the mean of the 8 - to 256 km curves in Figures 1*a* and 1*b*. Maximum likelihood estimates for the parameter α were found to be α=0.63±0.035 and α=1.66±0.37 for the visible and infrared data, respectively. The large difference in the maximum likelihood errors cited here is due at least in part to the fact that we directly estimate α' and $\Delta\alpha = (1+\alpha)^2\Delta\alpha'$; hence this effect alone accounts for a factor 2.7 in difference. Figures 1*a* and 1*b* show the best fit and mean visible and infrared curves. The standard errors in the fit are ±0.011 and ±0.015 respectively. These results show the accuracy of the graphical method. Using (13) and (14), we can also estimate h_d, γ_d. We find (using $d(A)$=2) $h_d \approx 13.80$, $\gamma_d \approx 3.50$ for infrared images, but for the visible data, $\max(C(h)) = 0.21/0.37 - 0.15 = 0.42 < 2$; hence there is no divergence. The large values estimated for h_d in infrared data show that the divergence would be difficult to detect directly: enormous samples would be needed.

4. THE CLASSICAL RADAR OBSERVER'S PROBLEM FOR MULTIFRACTAL REFLECTIVITY FIELDS

4.1. *Discussion*

The observer's problem for radar measurements of rain attempts to relate the observed ("effective") radar reflectivity factor (Z_{ob}) to more physically relevant parameters. In its classical form [*Marshall and Hitschfeld*, 1953; *Wallace*, 1953], it too makes assumptions of subsensor homogeneity (specifically that the rain drops have Poisson statistics over scales smaller than the radar "pulse volume": typically about 1 km^3). The variability in Z_{ob} is then considered to arise from two sources. The first is the natural variability of interest characterized by the reflectivity factor Z (proportional to the variance of the drop volumes). The second arises as a result of the random positions of each each of the drops within the pulse volume. Under certain assumptions about the homogeneity of the field and on the form of drop size distribution, Z can be related to the rain rate, total volume of liquid water, or other parameters of interest. The determination of Z from the observed Z_{ob} is therefore considered the basic "observer's problem" in radar meteorology.

Much work has been done to devise sampling and averaging strategies to obtain Z from Z_{ob}. In this section, we briefly review the standard derivation of the relation between Z and Z_{ob} and point out where it breaks down if the drops are distributed over sparse fractal sets rather than uniformly in space. We then show that if the latter effect is ignored, but that the Z field is multifractal, the observed codimension function $c_{ob}(\gamma)$ (for Z_{ob}) is identical to the underlying $c(\gamma)$ (for Z) in the limit where the natural variability builds up over a sufficiently wide range of scales (i.e., that the radar resolution is much smaller than the outer scale of the rain-producing processes). In other words, in this limit the natural variability is so strong that it completely dominates that arising from random fluctuations due to drop phases. This answers the question raised by *Zawadzki* [1987] as to which variability is strongest.

Although in this limit (at least as far as estimating $c(\gamma)$ is concerned) the observer's problem disappears, applications may require corrections. This is because the large parameter in the theory is the natural log of the range in scales ($\zeta=\ln\lambda$): taking a typical radar resolution of 1 km, and an external scale for the rain processes at 1000 to 10,000 km, we find ζ in the range ln (1,000) to ln (10,000) ≈7 - 9, which is not so large. In practice, corrections to the above will occur and the relation between $c_{ob}(\gamma)$ and $c(\gamma)$ will be more complex: we estimate these

corrections up to first order in $1/\zeta$. We then discuss the consequences of these findings in the light of some recent empirical studies of radar reflectivities by A. Seed et al.,(manuscript in preparation, 1990).

4.2. *Review of the standard approach*

Consider a radar at the origin that emits a pulse of electromagnetic waves that fills a volume υ at range r containing $n(\upsilon)$ scattering rain drops. Taking into account the various electrical, antenna, and other geometrical factors, the radar measures the effective reflectivity factor

$$Z_{ob} \propto |A|^2 \tag{19}$$

where

$$A = \sum_{j}^{n(\upsilon)} V_j e^{i\phi_j} \tag{20}$$

The sum is over all the drops in the volume, the V_j arises because the cross section of each drop is proportional to V, since water is polar molecule. The phases $\phi_j = 2\mathbf{k}\cdot\mathbf{r}_j$ where $\mathbf{k}$ is the radar wave vector, $\mathbf{r}_j$ the position of the drop, and the factor 2 arises because the beam must make a round trip. It is now customary to introduce the radar reflectivity factor, denoted Z (usually measured in units of mm^6/m^3), defined by

$$Z \propto n(\upsilon) \langle V^2 \rangle \tag{21}$$

The standard approach now assumes that all the $\mathbf{r}_j$ (and hence ϕ_j) are independent, and that $\langle V^2 \rangle$ is finite. Under these incoherent scattering assumptions, each term in the sum A is independent, the variances add, yielding $Z \propto n(\upsilon)$. Furthermore, by applying the central limit theorem, we can obtain the conditional probability distribution of Z_{ob} given Z:

$$p(Z_{ob}|Z) = \frac{1}{Z} e^{-Z_{ob}/Z} \tag{22}$$

This is the standard formula for the fluctuations in Z_{ob} due to random drop phases.

4.3. *Corrections due to multifractal reflectivity factors*

We have deliberately gone through the derivation in some detail in order to see exactly where the assumption of subsensor homogeneity is required. If the distribution of drops is fractal (as indicated by blotting paper analyses reported by *Lovejoy and Schertzer* [1990b], then the drops cluster and $n(\upsilon) \propto \upsilon^{d/3}$, where $d<3$ is the fractal dimension of the drop distribution (actually, horizontal cross sections were studied, yielding d(horizontal) $=1.82$). This clustering means that the ϕ_j are correlated, giving rise to some degree of coherent scattering. The effect of the coherent scattering is to make the modulus $\langle |A|^2 \rangle \propto n(\upsilon)^{2H}$ with $2H>1$ (*Lovejoy and Schertzer* [1990b] empirically find $2H \approx 1.24$). The combined effects of $d<3$, $2H>1$ lead to systematic corrections, so that Z_{ob} can no longer be directly regarded as an estimate of Z (see *Lovejoy and Schertzer* [1990b] for details). Presumably, it also leads to corrections in the above probability distributions, although empirical investigations would require much more data than used in the study cited. In the following, we ignore these subresolution fractal effects, concentrating our attention on the effect of the standard drop phase fluctuations on $c(\gamma)$.

We seek to express the observed $c_{ob}(\gamma_{ob})$ in terms of the true $c(\gamma)$, and ultimately to express the latter in terms of the former. Define

$$Z = \lambda^{\gamma} = e^{\zeta\gamma} \quad Z_{ob} = \lambda^{\gamma_{ob}} = e^{\zeta\gamma_{ob}} \tag{23}$$
$$p(\gamma) = \lambda^{-c(\gamma)} \quad p_{ob}(\gamma_{ob}) = \lambda^{-c_{ob}(\gamma_{ob})}$$

Now, using the formula for conditional probabilities, we obtain

$$p_{ob}(\gamma_{ob}) = \int p(Z_{ob}(\gamma_{ob})|Z)\, dZ \tag{24}$$

Substituting our definitions from above, and (22) for the conditional probability, we obtain

$$e^{-\zeta c_{ob}(\gamma_{ob})} = \int e^{-(e^{\zeta(\gamma_{ob}-\gamma)} + \zeta c(\gamma))} d\gamma \tag{25}$$

Using the standard method of steepest descent to estimate the value of this integral;

$$\zeta c_{ob}(\gamma_{ob}) = \min_{\gamma} (e^{\zeta(\gamma_{ob}-\gamma)} + \zeta c(\gamma)) \tag{26}$$

The minimum occurs when the following condition is satisfied:

$$c'(\gamma) = e^{\zeta(\gamma_{ob}-\gamma)} \tag{27}$$

Hence, when $\zeta \to \infty$, we obtain $\gamma_{ob} \to \gamma$, and $c_{ob}(\gamma_{ob}) \to c(\gamma)$, i.e., the observer's problem disappears, since the natural fluctuations are far larger than those introduced by the radar measurements. (The exceptional case $c'<0$ which can only occur for $\alpha=2$, $\gamma<\gamma_0$ yields exponential behavior and will not be discussed further).

However, realistic values of ζ are likely to be in the range 7-9, which is not so large. It is therefore of interest to estimate corrections due to the finite range of scales. To do this, it is convenient to introduce the small correction $\Delta/\zeta = \gamma - \gamma_{ob}$ and to solve (27) to first order in $1/\zeta$, (yielding $\Delta \approx \ln c'(\gamma_{ob})$). Defining the correction $\Delta c(\gamma) = c(\gamma) - c_{ob}(\gamma)$ and after a bit of algebra, we obtain

$$\Delta c(\gamma) = \frac{c'(\gamma)(\ln c'(\gamma) - 1)}{\zeta} + 0\left(\frac{1}{\zeta^2}\right) \tag{28}$$

Since $d\Delta c/dc' = \ln c'$, Δc has a minimum value of $-1/\zeta$ when $c'=1$, and a maximum value

$$\max(\Delta c(\gamma)) = \frac{h_d(\ln h_d - 1)}{\zeta} \tag{29}$$

where $h_d = c'(\gamma_d)$ is the maximum of $c'(\gamma)$ discussed earlier. Furthermore, the straight line asymptote of $c(\gamma)$ for $\gamma > \gamma_d$ is preserved; there is only a shift in the starting point to higher values of γ: $\gamma_{dob} \approx \gamma_d + (\ln h_d)/\zeta$ as well as a shift in the values of the codimensions of $h_d(\ln h_d - 1)/\zeta$. Since the straight line asymptote corresponds to the algebraic tail of the probability distribution, the above result is simply interpreted to mean that the exponent of the latter is conserved by the weaker (exponential) reflectivity fluctuations.

We can now estimate the effect of the above corrections if the graphical method outlined in section 3.2 is used to estimate the parameters. Since the correction is $-1/\zeta$ when the slope is $c'=1$, and this point is used to estimate C_t, γ_t, we have $C_t = C_{tob} - 1/\zeta$, $\gamma_t = \gamma_{tob} - 1/\zeta$, and corrections for c_0 being much smaller. Using

A. Seed et al.'s data (manuscript in preparation, 1990), we can estimate the maximum size of these corrections at the extreme large γ end, since empirically, they find that $3<\max(c')<3.5$ for the four meteorological situations studied over Montreal. Using the largest of these, and the smallest likely ζ (≈ 7), we obtain a maximum correction of 0.14. It should be noted that these corrections only apply to raw radar data, not data that have been artificially degraded in resolution by averaging Z_{ob}, as in A. Seed et al. (manuscript in preparation, 1990) for resolutions 4 km and greater. In the latter case, the true correction is likely to be smaller, although this mixture of averaging at subradar resolution in Z and at larger resolution in Z_{ob} is not easy to analyze.

Once we have obtained an estimate for $c(\gamma)$ for the reflectivity factor, the corresponding function for the rain rate can be obtained by the linear tranformation $\gamma \rightarrow B\gamma$ (see section 2.2).

5. CONCLUSIONS

The extremely variable nature of rain and cloud fields over wide ranges of scale typically implies that remote measurements of the fields involve sensor resolutions much larger than the smallest scale of the variability. These data will therefore contain (potentially strong) resolution dependencies. It has been suggested for some time, on both theoretical and empirical grounds, that over considerable ranges, these fields exhibit scaling fractal (and more recently, multifractal) structures. In multifractal systems, a resolution-independent function exists (the codimension function $c(\gamma)$) which is essentially an (appropriately normalized) probability distribution, which characterizes the statistical properties of the field over the entire scaling range and can be measured by observers using instruments at widely differing scales (it is therefore useful in calibration). These codimension functions are themselves expected to be determined by three dynamically important parameters (determining the "universality classes"), thus considerably simplifying the analysis and modeling of such fields. A relevant point to note here is that the universality classes are readily compatible with lognormal phenomenologies.

In this paper, we reexamined some earlier analyses. Some (which we termed monofractal) used methods primarily designed for studying fields characterized by a single fractal dimension. In appendices, we discuss at a fairly technical level some of the problems that arise when such methods are applied to multifractals. We also reviewed some of the recent developments in the field of multifractals indicating some of their basic proerties and outlined a new technique [*Lavallée et al.*, 1990] for empirically estimating $c(\gamma)$ called the probability distribution /multiple scaling (PDMS) technique, applying the method to satellite cloud data at both visible and infrared wavelengths. In a final section, we showed how radar estimates of $c(\gamma)$ can be corrected for the classical effect of "drop randomization" in order to determine $c(\gamma)$ for the radar reflectivity factor (Z) from the measured effective radar reflectivity factor. We then indicated how the latter can be used to obtain the corresponding function for the rain rate via a linear transformation of the orders of singularities of Z. We discussed these results in comparison with the empirical $c(\gamma)$ measured by A. Seed et al. (manuscript in preparation, 1990).

APPENDIX A: THRESHOLDING AND MULTIFRACTAL MEASURES REEVALUATION OF SEVERAL MONODIMENSIONAL ANALYSIS TECHNIQUES

A.1 Discussion

We have argued (especially in section 2) that emphasis on the geometric properties of scale invariant processes has lead to excessive emphasis on the study of sets and their fractal dimensions. For example, using a threshold on satellite cloud and radar rain data, *Lovejoy* [1981, 1982] determined area-perimeter and area-distribution exponents. Although limited to the range 1-1000 km, and to a single cloud and rain intensity level and meteorological situation, *Lovejoy* [1982] showed that scaling could hold over a wide range of meteorologically significant length scales. Since then, these and related methods have been used by a number of other investigators [e.g., *Carter et al.*, 1986; *Ludwig and Nitz*, 1986; *Rhys and Waldvogel*, 1986; *Welch et al.*, 1988; and *Cahalan*, 1990], occasionally yielding apparently contradictory results. For example, the value of the area-perimeter exponent of 1.35 found in *Lovejoy* [1982] was at first considered a fundamental constant, which was subsequently found to be not always reproducible; *Rhys and Waldvogel* [1986] and *Cahalan* [1990] found generally higher values that depended on the realization ("meteorological situation"), and *Carter et al.* [1986] estimated the dimension of the "graph" of infrared radiance intensity from clouds, obtaining yet another value of the dimension. However, once the multifractal nature of the fields is appreciated, these results can be easily explained. In particular, the interpretation and significance of the area-perimeter and area distribution exponents, graph dimensions, as well as their relationship to the fractal dimensions of the rain or cloud regions themselves must be reexamined. This is done below; the most important results are (1) the area-perimeter exponent will in general not be equal to the fractal dimension of perimeter, and (2) the range of possible values and significance of the area distribution exponent is different than that obtained by simple arguments on geometric sets. We then reexamine these early studies in this multifractal context.

A.2. Multifractal Exceedance Sets, Perimeter Sets, and Graphs

Consider the function $f_\lambda(\mathbf{r})$ obtained by averaging a multifractal measure over scale ratio $\lambda=L/\eta$ where η is the inner scale of the variability, in a region of the plane $\Re$ size $R\times R$ (generalizations to higher dimensional spaces are straightforward and will not be explicitly considered). As mentioned in section 2, the underlying measure is most directly studied by considering how the properties of f_λ vary as we change λ (e.g., by successively degrading our sensor resolution). However, most applications of remotely sensed data involve studying the properties of f_λ at fixed λ. When, as is often the case, these exponents are obtained by using thresholds (T) on f_λ to define sets, we find that the results will depend directly on λ via the multifractal relation $T=T_I\lambda/\lambda_I)^{-\gamma}$, where T_I is the large (e.g., image) scale resolution value of the field (T_I is the same as $f_{\lambda I}$ in section 2). Our exponents will therefore depend (via T) on both the sensor resolution (λ), and the meteorological situation (i.e., stochastic realization) of the process, and hence be of limited utility. Below, we fix the function resolution L, and write simply $f(\mathbf{r})$.

Define the (closed) exceedance set $S_{T\geq}$ as the set of points satisfying $f(\mathbf{r}) \geq T$. If $f(\mathbf{r})$ is a scaling function, the (Hausdorff) dimension $D(S_{T\geq})$ of $S_{T\geq}$ will be a nonincreasing function of T, since $S_{T\geq} \supset S_{T'\geq}$ for $T'>T$ and the dimension of a subset must less than or equal to the dimension of the entire set (this property is so basic that it holds for all definitions of dimension of which we are aware, including topological dimensions). Complications arising from non-self-similar, anisotropic scaling (generalized scale invariance, [e.g., *Schertzer and Lovejoy*, 1987*a*, *b*]), will not be considered here.

Consider next the "graph" (G) of $f(\mathbf{r})$ defined as those points in three-dimensional $(\mathbf{r}, f(\mathbf{r}))$ space. As before, we may define G_T as the subset of G such that $f(\mathbf{r})\geq T$ (see Figure A1 for an illustration, and appendix B.2 for more discussion). Consider

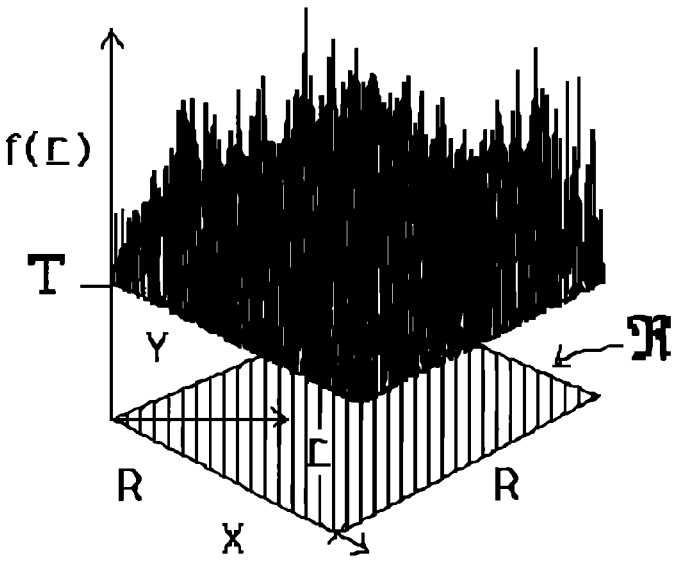

Fig. A1*a*. Schematic illustration showing some of the definitions used in the text. G_T is the set of points in the black spiky region above the plane ($f(\mathbf{r})=T$).

now the perimeter set of $S_{T\geq}$, denoted p_T; p_T is the "border set" of $S_{T\geq}$, more properly defined as the "T-crossing set" of G with the plane $f(\mathbf{r})=T$ (in analogy with the expression "zero-crossing" used in the theory of stochastic processes). This is the set of points $\mathbf{r}$ such that arbitrarily small neighborhoods of $\mathbf{r}$ contain some points such that $f(\mathbf{r})<T$ and some such that $f(\mathbf{r})\geq T$. Using basic notions about sets, we can now give a definition of p_T. Define the (open) complement of $S_{T\geq}$ as: $\overline{S}_{T\geq} = \Re - S_T$; p_T is thus the set of "contact" points of $\overline{S}_{T\geq}$ which are required to close it, yielding $[\overline{S}_{T\geq}]$. We thus obtain

$$p_T = [\overline{S}_{T\geq}] \cap S_{T\geq} \tag{A1}$$

It is important not to confuse this zero-crossing set with the set of points $\mathbf{r}$ such that $f(\mathbf{r})=T$, which is the intersection of G with the plane $f(\mathbf{r})=T$, ($G\cap T$) denoted $S_{T=}$. In general, p_T will be different from $S_{T=}$ with the two coinciding only if special conditions apply such as G is everywhere continuous (i.e., if G rarely jumps from one side of the plane $f(\mathbf{r})=T$ without intersecting it); $p_T = S_{T=}$ does, however, generally apply to the mono-dimensional processes such as fractional Brownian motion discussed by *Mandelbrot* [1982]. However, in what follows, we see that in general, G is discontinuous, and all we obtain is

$$D(S_{T\geq}) \geq D(p_T) \tag{A2}$$

(since $S_{T\geq} \supset p_T$) with the actual value of $D(p_T)$, however, depending critically on the topological structure (i.e., connectedness) of the set. Figure A1*c* compares the functions $D(S_{T\geq})$, $D(p_T)$, $D(S_{T=})$ for a numerical simulation of a multifractal cascade process on a 128X128 point grid (mean of 1), with Gaussian generator (except for the extreme fluctuations, the intensities are lognormally distributed; see *Lavallée et al.* [1990] for more details). The dimensions were estimated using box counting. In order to get a large enough sample size to estimate the dimension function $D(S_{T=})$, the latter was estimated from the sets $S_{T+\Delta T\geq}$-$S_{T>}$ with $\Delta T=0.2T$.

Note that as $T\rightarrow\infty$, $D(S_{T\geq})$ can $\rightarrow D_\infty > 0$, although in general (especially in continuous cascades), we expect $D_\infty = 0$. In the latter (more general) case, $D(p_T)$ may initially increase with T, although it must eventually decrease.

A.3. The relation between $D(p_T)$ and area-perimeter exponents

We can now relate the areas and perimeters by eliminating R in the above equations. Using box counting to estimate the Hausdorff dimensions, we obtain

$$N_S(r) \approx \left(\frac{R}{r}\right)^{D(S_{T\geq})} \tag{A3}$$
$$N_p(r) \approx \left(\frac{R}{r}\right)^{D(p_T)}$$

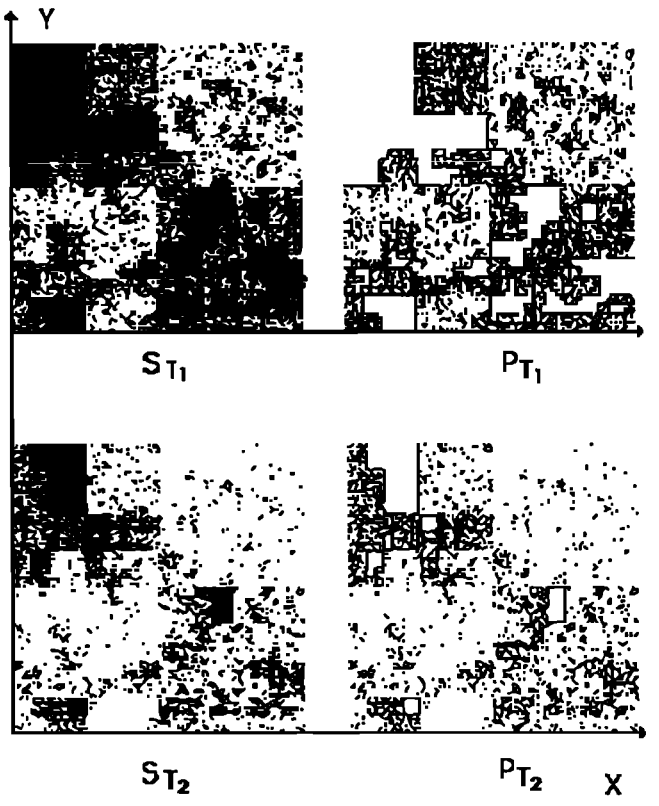

Fig. A1*b*. Schematic illustration showing the definition of $S_{T\geq}$, p_T used in the text, for two different thresholds $T_1<T_2$. The illustration was produced using a multiplicative cascade process (an "alpha model") with a cascade discretized into eight steps with a scale factor 2 in each step.

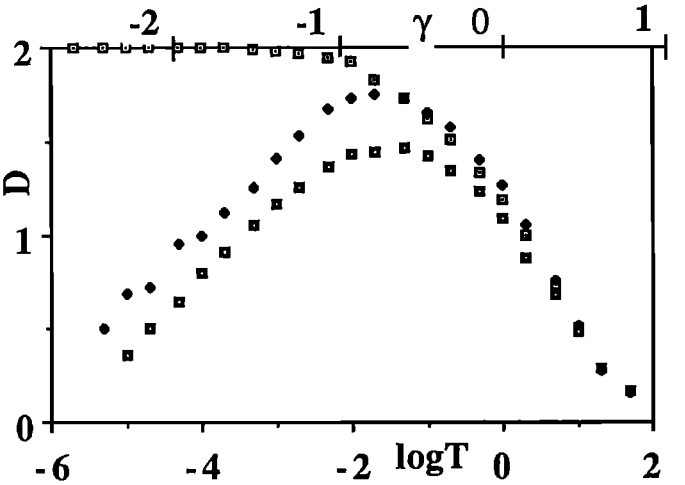

Fig. A1*c*. Graph of the functions $D(S_{T\geq})$ (white squares), $D(p_T)$ (diamonds), $D(S_{T=})$ (solid squares) determined numerically from a multiplicative cascade process on a 128 X 128 point grid. As expected, the functions respect the inequality (A2).

where N is the number of rXr boxes required to cover the set (which is of linear size R).

The areas $A_T(r)$ and perimeters $P_T(r)$ are given by

$$A_T(r) = N_S(r)r^2 = \left(\frac{R}{r}\right)^{D(S_{T\geq})} r^2 \qquad (A4)$$

$$P_T(r) = N_P(r)r = \left(\frac{R}{r}\right)^{D(p_T)} r$$

eliminating R, we obtain

$$P_T = A_T^{D(p_T)/D(S_{T\geq})} r^{1-2D(p_T)/D(S_{T\geq})} \qquad (A5)$$

or:

$$P \propto (\sqrt{A})^{\xi_T} r^{1-\xi_T} \qquad (A6)$$

where $\xi_T = 2D(p_T)/D(S_{T\geq})$. When $D(S_{T\geq})=2$ (i.e., the exceedance sets are not fractal), we obtain $\xi_T = D(p_T)$, which is the relationship discussed by *Mandelbrot* [1982], and applied to cloud areas by *Lovejoy* [1982]. Alternatively, using the value ξ_T rather than $D(p_T)$, we are in error by the ratio $2/D(S_{T\geq}) \geq 1$.

Recently, *Welch et al.* [1988] used the same method to analyze LANDSAT data with 28 m resolution to study visible cloud radiance fields. Although the authors claim that two straight lines with slightly different slopes (what they call "bifractal" behavior) can be fit to their graphs (with a break at about 1 km^2), single straight lines (one for each scene) do excellent jobs, as readers may verify for themselves (see Figure A2 reproduced from their Figure 8). In any case, since these authors applied their analyses to single scenes, there will be statistical fluctuations due to the finite sample size. Furthermore, basic theoretical ideas about multifractals (as well as cascade simulations performed by *Lavallée et al.* [1990]) indicate that for multifractal fields, fluctuations will generally be very large (strong intermittency) from one realization to another. In any case, it would be interesting (following *Gabriel et al.* [1988]) for the authors to reanalyze their data to try (for each scene seperately) to statistically reject the hypothesis that individual straight provide good fits. For the moment, we interpret these data as giving strong support for the scaling of cloud radiance perimeters between 10^{-2} and 10^4 km^2 for a variety of cloud types (i.e., precisely through the range of 1 km^2 where *Cahalan* [1990] claims evidence for a break).

The above analysis shows that we should not be surprised by the empirical finding that area-perimeter relations give fairly constant exponents typically in the range $1.3 \leq \xi_T \leq 1.6$, since both $D(p_T)$ and $D(S_{T\geq})$ are likely to decrease slowly with increasing T, and hence the ratio $D(p_T)/D(S_{T\geq})$ may be expected to remain relatively fixed (see *Yano and Takeushi* [1990] and *Cahalan* [1990]; the latter finds a slight increase of ξ_T with T, yielding typical low (dim) cloud values of 1.5, and high (bright) cloud values of 1.6). Note that this correction is not negligible; empirically, we find (section 3 and *Gabriel et al.* [1988]) that even for very low values of T, $D(S_{T\geq}) \approx 1.8$ at both visible and infrared wavelengths, and may easily decrease to $\approx$1.5 for very bright regions or cold tops. These values lead to corrections of 1.11 and 1.33, respectively. Applying these to Cahalan's typical range of ξ_T values we obtain $D(p_T) \approx 1.35$ and 1.20, respectively.

A.4. Other implications of multifractals, For analysis methods

The preceding subsections have shown that multifractal fields are generally considerably more difficult to analyze than their monodimensional counterparts. Two other techniques that have been used to study scaling in cloud fields are area distribution exponents and the dimensions of graphs. Both techniques must be applied with considerable care to multifractal fields. In the former case (discussed in detail in appendix B) the interpretation of the exponents is quite different for multifractal and monofractals. In the latter, shortcuts in performing box counting that assume continuity of the process (which holds in many common monofractal processes but not generally in multifractal ones) can (and do) lead to erroneous results.

Another aspect of multifractals that must be carefully considered in analyzing data is that unlike the monodimensional case, the thresholds that correspond to a given fractal dimension depend directly on the resolution with which the basic fractal measure is averaged by the measuring device. Even if the resolution is constant, the dimension corresponding to a given threshold will also depend on the realization of the process (e.g. the meteorological situation). As argued earlier, this difference between monofractal and multifractal processes is very basic; for now, we briefly discuss how these new dependencies can lead to practical difficulties, including apparent breaks in the scaling symmetry.

Pooling data from different realizations. Pooling data (e.g., in box counting, in area-perimeter graphs, or in area histograms) is a useful way of increasing sample size to obtain better statistical estimates of the parameters. However, it must be performed carefully in multifractal fields, since it can "mix" fractals with different dimensions. For example, *Rhys and Waldvogel* [1986] consider area-perimeter relations obtained by pooling areas and perimeters of radar rain areas over consecutive images in time, using the same threshold. Since the dimensions for the fixed threshold will in general vary in time, this mixes fractals with different dimensions. If the sample was large enough, this would not be serious, since the largest area-perimeter exponent would eventually dominate the rest. However, if the fractals have nearly the same dimensions (as they do in their study), the convergence is extremely slow, and finite samples will yield either large spreads or nonlinear log-log plots that can easily (and erroneously) be interpreted as breaks in the scaling. These results must therefore be reanalyzed before any conclusions about symmetry breaking can be drawn.

Combining spatial averaging with thresholding. The variation of fractal dimension with threshold can lead to artificial symmetry breaking in yet another way. Consider taking a shortcut in estimating areas and dimensions by fixing a threshold and degrading successively the resolution of the set which exceeds the threshold (e.g., by box counting), calculating p_T from the set at different resolutions. This method will work whether or not the field is multifractal, since it is first converted into a set having a well-defined dimension. However, if rather than degrading the set resolution, we degrade the multifractal field itself by simply averaging the field (rather than the set) over larger and larger scales, and then defining the exceedance set with respect to the previous threshold (as in *Yano and Takeuchi* [1990]), the method will no longer work. To recuperate a set with the same dimension, the threshold must be appropriately decreased to compensate for the fact that averaging over larger scales decreases (smooths) the intense regions (the precise amount of decrease can be quantitatively estimated by associating each threshold with singularities as in the following section). As long as the thresholds used are sufficiently low that the dimension varies relatively little with threshold (i.e., in this range of thresholds, the field is approximately monodimensional), this effect will not be too important, but at extreme threshold levels, where the dimension changes more rapidly with threshold (e.g., for the cirrus clouds in *Yano and Takeuchi* [1990]), this will yield systematic (but totally artificial) breaks in the scaling (the downward curvature observed in their curves).

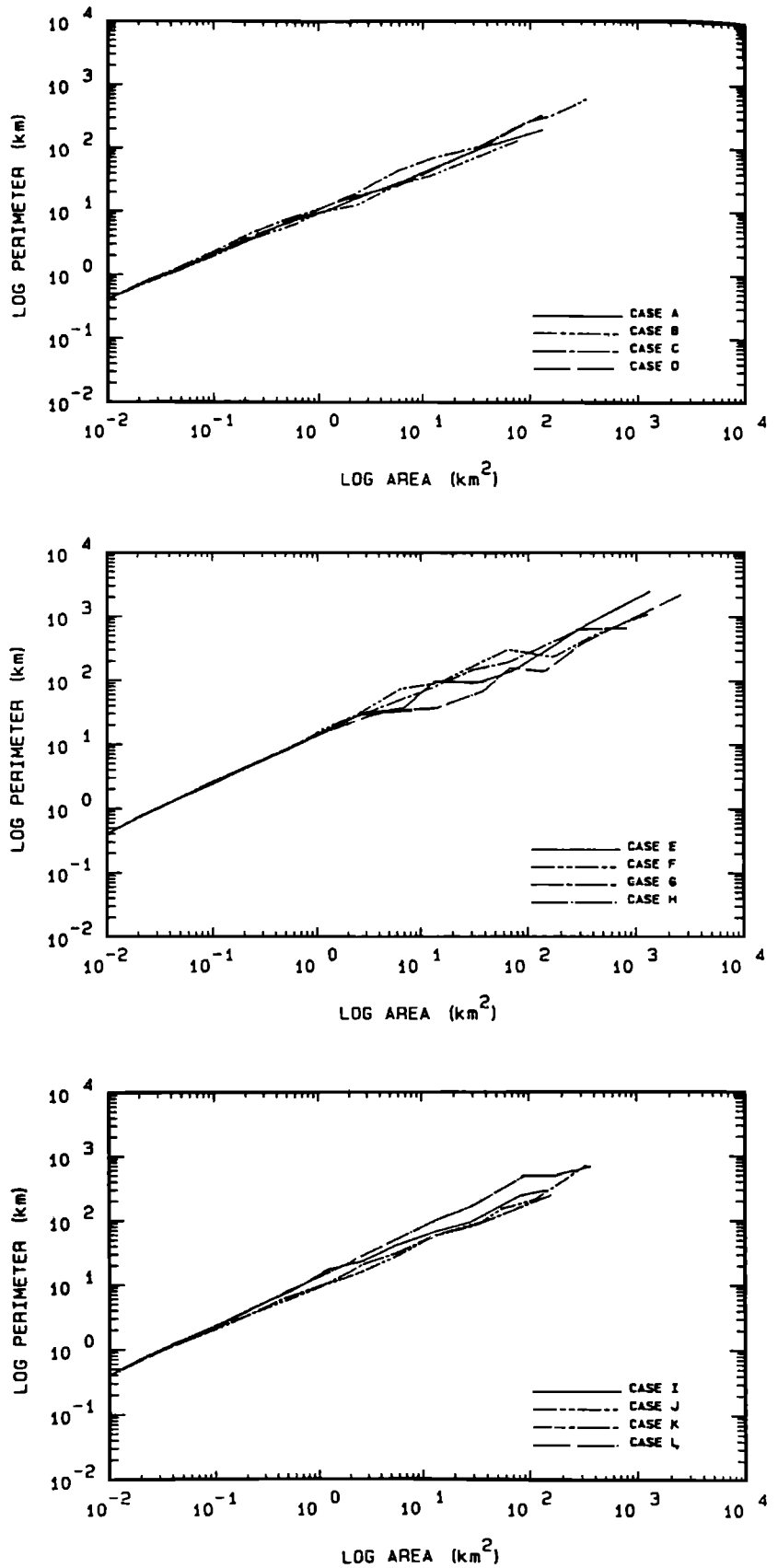

Fig. A2 Area-perimeter curves for nine different LANDSAT scenes (28 m resolution) reproduced from *Welch et al.* [1988]. Although, as expected, different scenes yield different slopes, there is no evidence for a break in the scaling over the entire range of 10^{-2} to 10^4 km^2.

APPENDIX B: OTHER PRIMARILY MONODIMENSIONAL ANALYSIS TECHNIQUES

B.1. Area distribution exponents

Consider the problem of relating the distribution of contiguous areas equal to or exceeding T to the set $S_{T\geq}$. If $D(S_{T\geq}) > 1$, then $S_{T\geq}$ will generally be made up of many contiguous subsets (denoted $s_{T\geq}^{(i)}$), each with external scale Λ_i for the i^{th} region. Because of the assumed scaling, the Λ will generally be distributed (to within logarithmic corrections) as

$$\mathrm{Nr}(\Lambda>L) \propto L^{-B_T} \tag{B1}$$

where Nr indicates the number of subsets $s_{T\geq}^{(i)}$ whose size exceeds L. Note that since $S_{T\geq} \supset s_{T\geq}$, $D(s_{T\geq}) \leq D(S_{T\geq})$.

At resolution r, a subset $s_{T\geq}$ with scale L will have area

$$a_T(r) \approx \left(\frac{L}{r}\right)^{D(s_{T\geq})} r^2 \tag{B2}$$

Hence, eliminating L in terms of a_T, we obtain

$$\mathrm{Nr}(A_T>a_T) \propto a_T^{-B'_T} \tag{B3}$$

where $B'_T = B_T/D(s_{T\geq})$. Empirically, B'_T is the most readily accessible area exponent. *Lovejoy [1981]*, and *Lovejoy and Mandelbrot* [1985] show empirically that for light rain rates, low clouds, $B'_T \approx 0.75$. *Lovejoy and Mandelbrot* [1985] and *Lovejoy and Schertzer* [1985] also develop monodimensional models with B'_T in the range 0.5-0.75. Another reference is *Cahalan* [1990], who obtains $B'_T \approx 0.8$ for satellite cloud pictures.

We now seek to relate B_T, $D(s_{T\geq})$ and $D(S_{T\geq})$. To do so, note that the total number of boxes required to cover S_T is

$$N_S(r) \approx \left(\frac{R}{r}\right)^{D(S_{T\geq})} \propto \int_r^R \left(\frac{L}{r}\right)^{D(s_{T\geq})} d\mathrm{Nr}(L>L) \tag{B4}$$

where $d\mathrm{Nr}(\Lambda>L) \propto L^{-B_T-1}dL$ is the number density associated with $\mathrm{Nr}(\Lambda>L)$. The above yields

$$N_S(r) \propto r^{-D(s_{T\geq})} \int_r^R L^{D(s_{T\geq})} L^{-B_T-1} dL \tag{B5}$$

taking into account the sign of $D(s_T) - B_T$, this yields

$$N_S(r) \propto r^{-D(s_{T\geq})} \left[\left| R^{D(s_{T\geq})-B_T} - r^{D(s_{T\geq})-B_T} \right| \right] \tag{B6}$$

The relative values of $D(s_{T\geq})$ and B_T depends on the topological (connectedness) properties of the process. We must now distinguish two cases depending on which is greater:

For the case $B_T \geq D(s_{T\geq})$. In this case, in the limit $r \to 0$, the $r^{D(s_{T\geq})-B_T}$ term dominates the $R^{D(s_{T\geq})-B_T}$ term and the number of boxes/subset is small compared with the total number; fragmentation dominates, and

$$N_S(r) \propto r^{-B_T} \quad \Rightarrow \quad B_T = D(S_{T\geq}) \tag{B7}$$

This is the case discussedby *Mandelbrot* [1982], where geometric generators are used to produce fractal sets which yield $D(s_{T\geq}) < D(S_{T\geq})$. We therefore have $D(S_{T\geq}) = B_T > D(s_{T\geq}) \Rightarrow B'_T = B_T/D(s_{T\geq}) > 1$.

For the case $B_T \leq D(s_{T\geq})$. In this case, in the limit $r \to 0$, $R^{D(s_{T\geq})-B_T}$ dominates $r^{D(s_{T\geq})-B_T}$ and the number of boxes/fractal subset is a large fraction of the total; the number of boxes needed to cover the fragments is negligible compared with the number needed to cover individual connected regions, this yields:

$$N_S(r) \propto r^{-D(s_{T\geq})} \quad \Rightarrow \quad D(s_{T\geq}) = D(S_{T\geq}) \tag{B8}$$

and $B_T < D(s_{T\geq})$ and hence $B'_T = B_T/D(s_{T\geq}) < 1$. Each contiguous region has the same dimension as the entire set, and the fragmentation is relatively unimportant. This is the case relevant to multifractal fields and of interest in geophysical applications.

B.2 Graphs and their dimensions

Carter et al. [1986] considered the x-z cross section (intersection) of the graph G of the infrared cloud radiance as a function of telescope scanning angle (for clarity, we use the notation $(\mathbf{r}, f(\mathbf{r})) = (x,y,z)$ since $\mathbf{r} = (x,y)$ and $f=z$=radiance, x,y are angle variables). Denote this intersection set by $G \cap (xz)$. They then estimate the dimension of G using boxcounting to cover the graph of $G \cap (xz)$. However, their method actually implicitly assumes continuity; they use additional boxes to cover not only their experimental points, but also those points on straight lines connecting the latter. Their resulting estimate of $D(G \cap (xz))$ is very near 1 (1.16 and 1.11, depending on the wavelength used), and we may therefore suspect that it is an artifact of their assumption of continuity (since the connecting straight lines have dimension 1, while the experimental points have $D<1$, their method will estimate the maximum of the two). We now discuss this possibility in more detail.

The simplest way to relate $D(G_T)$ to $D(S_{T\geq})$ and $D(S_{T=})$ is to recall that $S_{T\geq}$ is the projection of G_T with the x,y plane. The projection set (S_p) of S_1 onto S_2 has dimension

$$D(S_p) = \min(D(S_1), D(S_2)) \tag{B9}$$

which is a basic property of projections. In this case, we obtain

$$D(S_{T\geq}) = \min(D(G_T), 2) \tag{B10}$$

There are now two distinct possibilities.

For the case $D(S_{T\geq})=2$. If the process is nonstationary, such as the (monodimensional, Gaussian) fractal Brownian motion processes used by *Mandelbrot* [1982] and *Voss* [1983] to model mountains, then the graph is continuous (but nondifferentiable) but rarely crosses the plane $f(\mathbf{r})=T$, and $D(S_{T\geq})=2$, and the projection relation gives us no further information about $D(G_T)$.

For the case $D(S_{T\geq})<2$. The process is stationary (as are cascade processes and, presumably, most remotely sensed fields); in this case we will generally have $D(S_{T\geq})<2$, and hence the projection relation yields

$$D(G_T) = D(S_{T\geq}) < 2 \tag{B11}$$

In this case (which applies to the examples shown in Figures A1*a*-A1*c*), G_T will be discontinuous everywhere. We now consider $G \cap (xz)$ studied by *Carter et al.* [1986]. All the preceding results apply to $G \cap (xz)$, $S_{T\geq} \cap (xz)$, etc., as long as the dimensions of all the above sets are reduced by one (if the corresponding value becomes negative, it must be reset to zero). Since we have empirical evidence that generally $D(S_{T\geq})<2$ (see section 2), we expect $D(S_{T\geq}) = D(G_T)$, so that $D(G_T \cap (xz)) = D(S_{T\geq} \cap (xz)) < 1$, implying that $G \cap (xz)$ is discontinuous everywhere. However, *Carter et al.* [1986] assumed that $G \cap (xz)$ was continuous and effectively interpolated their experimental points with a continuous line (dimension 1, which

is > $D[G\cap(xz)]$]); hence we expect them to obtain an estimate D=1 (the maximum of the dimension of the set of points on $G\cap(xz)$ and the set on the line connecting them). Indeed, careful inspection of the *Carter et al.* [1986] box-counting figures ($N(L)$ versus L) indicate that the function $N(L) \approx L^{-1}$ (hence $D = 1$) fits well over most of the range of L (which was only over roughly 2 orders of magnitude anyway).

This example illustrates the dangers of approaching the data analysis with unwarranted theoretical preconceptions about the continuity of the process.

Acknowledgments. We acknowledge discussions with G.L. Austin, A. Davis, P. Gabriel, J.P. Kahane, P. Ladoy, D. Lavallée, E. Levich, A. Seed, A.A. Tsonis, R. Viswanathan, and J. Wilson.

REFERENCES:

Benzi, R., G. Paladin, G. Parisi, and A. Vulpiani, *J. Phys. A, 17*, 3521, 1984.

Cahalan, R.F., Landsat observations of fractal cloud structure, in *Scaling, Fractals and Non-Linear Variability in Geophysics*, edited by D. Schertzer and and S. Lovejoy, Kluwer, Holland, in press, 1990.

Carter, P.H., R., Cawley, A. L. Licht, M.S. Melnik, *Dimensions and Entropies in Chaotic Systems*, edited by G. Mayer-Kress, pp. 215-221, Springer, New York, 1986.

Drufuca, G., Radar derived statistics on the structure of precipitation patterns, *J. Appl. Meteorol., 16*, 1029-1035, 1977.

Fan, A., H., Chaos additif et multiplicatif de Lévy. *C. R. Acad. Sci. Paris 1, 308*, 151-154, 1989a.

Fan, A., H., Decomposition de de mesures et recouvrement aléatoire. *phD. thesis*, U. Paris Sud, 143pp, Nov. 1989b.

Frisch, U., and G. Parisi, A multifractal model of intermittency, in *Turbulence and Predictability in Geophysical Fluid Dynamics and Climate Dynamics*, edited by Ghil, Benzi, Parisi, pp 84-88, North-Holland, Amsterdam, 1985.

Feller, W., *An Introduction to probability theory and its applications, vol. 2*, Wiley, New York, 1971.

Gabriel, P., S. Lovejoy, D. Schertzer, and G.L. Austin, Multifractal analysis of resolution dependence in satellite in satellite imagery, *Geophys. Res. Lett., 15*, 1373-1376, 1988.

Grassberger, P., Generalized dimensions of strange attractors, *Phys. Lett. A, 97*, 227, 1983.

Halsey, T.C., M.H. Jensen, L.P. Kadanoff, I. Procaccia, and B. Shraiman, Fractal measures and their singularities: The characterization of strange sets, *Phys. Rev. A, 33*, 1141-1151, 1986.

Hentschel, H.G.E., and I. Proccacia, The infinite number of generalized dimensions of fractals and strange attractors, *Physica, 8D*, 435-444, 1983.

Houze, R.A., and C.-P. Cheng, Radar characteristics of tropical convection observed during GATE: Mean properties and trends over the summer season, *Mon. Weather Rev., 105*, 964-980, 1977.

Konrad, T.G., Statisitcal models of summer rainshowers derived from fine-scale radar observations. *J. Appl. Meteorol., 17*, 171-188, 1978.

Ladoy, P., D. Schertzer, and S. Lovejoy, Une étude d'invariance locale-regionale des temperatures, *La Meteorol., 7*, 23-34, 1986.

Lavallée, D. D. Schertzer, and S. Lovejoy, On the determination of the codimension function in *Scaling, Fractals and Non-Linear Variability in Geophysics*, edited by D. Schertzer and S. Lovejoy, Kluwer, Holland, in press, 1990.

Lopez, R. E., Some properties of convective plume and small fair-weather cumulus fields as measured by acoustic and lidar sounders, *J.Appl .Meteorol., 16*, 861-865, 1979*a*.

Lopez, R. E., The log-normal distribution and cumulus cloud populations, *Mon. Weather Rev. , 105*, 865-872, 1979*b*.

Lovejoy, S., Analysis of rain areas in terms of fractals, paper presented at the *20th Conference on Radar Meteorology*, Am. Meteorol. Soc., 1981.

Lovejoy, S., The area-perimeter relationship for rain and cloud areas, *Science, 216*, 185-187, 1982.

Lovejoy, S., and B. Mandelbrot, Fractal properties of rain and a fractal model, *Tellus, 37A*, 209-232, 1985.

Lovejoy, S., and D. Schertzer, Generalized scale invariance in the atmosphere and fractal models of rain. *Water Resour. Res., 21*, 1233-1250, 1985.

Lovejoy, S., and D. Schertzer, Scale invariance, symmetries fractals and stochastic simulation of atmospheric phenomena, *Bull Am. Meteorol. Soc., 67*, 21-32, 1986*a*.

Lovejoy, S., and D. Schertzer, Scale invariance in climatological temperatures and the spectral plateau, *Ann. Geophys., 4B*, 401-410, 1986*b*.

Lovejoy, S., and D., Schertzer, Multifractal analysis techniques and the rain and cloud fields from 10^{-3} to 10^{6}m, in *Scaling, Fractals and Non-Linear Variability in Geophysics*, edited by D. Schertzer, and S. Lovejoy, Kluwer, Holland, in press, 1990a.

Lovejoy, S., and D., Schertzer, Fractals, rain drops, and resolution dependence of rain measurements, *J. Appl. Meteor.* (in press), 1990b.

Lovejoy, S., D. Schertzer, and A.A. Tsonis, Functional box-counting and multiple elliptical dimensions in rain, *Science, 235*, 1036-1038, 1987.

Ludwig, F.L., and K.C. Nitz, Analysis of lidar cross sections to determine the spatial structure of material in smoke plumes. *Proceedings of Smoke Obscurants Symposium*, vol. 10, pp 231-241, Harry Diamond Labs., Adelphi, Md., 1986.

Mandelbrot, B., *The Fractal Geometry of Nature*, W.H. Freeman, 465 pp., New York, 1982.

Marshall, J.S., and W. Hitschfeld, Interpretation of fluctuating echoes from randomly distributed scatters, I., *Can. J. Phys., 31*, 962-994, 1953.

Rhys, F.S., and A. Waldvogel, Fractal shape of hail clouds, *Phys. Rev. Lett., 56*, 784-787, 1986.

Schertzer, D., and S. Lovejoy, On the dimension of atmospheric motions, paper presented at the *IUTAM Symposium on Turbulence and Chaotic Phenomena in Fluids*, Int. Union Theor. and Appl. Mech., 1983.

Schertzer, D., and S. Lovejoy, The dimension and intermittency of atmospheric dynamics, in *Turbulent Shear Flow, Vol. 4*, edited by B. Launder, pp. 7-33, Springer, New York, 1985*a*.

Schertzer, D., and S. Lovejoy, Generalized scale invariance in turbulent phenomena, *P.C.H. J., 6*, 623-635, 1985*b*.

Schertzer, D., and S. Lovejoy, Singularités anisotropes, et divergence de moments en cascades multiplicatifs. *Ann. Math. Que., 11*, 139-181, 1987*a*.

Schertzer, D., and S. Lovejoy, Physically based rain and cloud modeling by anisotropic, multiplicative turbulent cascades, *J. Geophys. Res. 92*, 9693-9714, 1987*b*.

Schertzer, D., and S. Lovejoy, Generalized Scale invariance and multiplicative processes in the atmosphere, *Pure Appl. Geophys., 130*, 57-81, 1989.

Schertzer, D., and S. Lovejoy, Nonlinear variability in geophysics: multifractal simulations and analysis, in *Fractals: physical origins and properties*, edited by L. Pietronero, Plenum press, New York, in press, 1990a.

Schertzer, D., and S. Lovejoy, Observables and universality classes for multifractal fields, in *Scaling, Fractals and Non-Linear Variability in Geophysics*, edited by D. Schertzer, and S. Lovejoy , Kluwer, Holland, in press, 1990*b*.

Schertzer, D., S. Lovejoy, R. Visvanathan, D. Lavallée, and J. Wilson, Universal Multifractals in Turbulence, in *Fractal Aspects of Materials: Disordered Systems*, Edited by D.A. Weitz, L.M. Sander, B.B. Mandelbrot, 267-269, Materials Research Society, Pittsburg, Pa., 1988.

Schertzer, D., S. Lovejoy, R. Visvanathan, D. Lavallée, and J. Wilson, Universal Multifractals in Turbulent Flows, paper presented at Nonlinear World, 4th International workshop on nonlinear and turbulent processes in physics, Kiev, 1989.

Shih, F.C., M. Wetzel, and T.H. Vonder Haar, Effects of data resolution on marine stratiform cloud detection using AVHRR and VISSR satellite data, paper presented at 3rd Conference on Satellite Meteorology and Oceanography, Am. Meteorol. Soc., Anaheim, Calif., 1988.

Voss, R., Fourier synthesis of Gaussian fractals: 1/f noises, landscapes and flakes, paper presented at the Siggraph Conference, Detroit, 1983.

Wallace,P.R., Interpretation of fluctuating echoes from randomly distributed scatters, II, *Can. J. Phys., 31*, 995-1009, 1953.

Warner, C., and G.L. Austin, Statistics of radar echoes on day 261 of GATE, *Mon. Weather Rev., 106*, 983-994, 1978.

Waymire, E., Scaling limits and self-similarity in precipitation fields, *Water. Resour. Res., 21*, 1251-1265, 1985.

Waymire, E., and V. K. Gupta, On scaling and log-normality in rainfall? in *Scaling, Fractals and Non-Linear Variability in Geophysics*, edited by D. Schertzer and S. Lovejoy, Kluwer, in press, 1990.

Welch, R.M., K.S. Kuo, B.A. Wielicki, S.K. Sengupta, and L. Parker, Marine stratocumulus cloud fields off the coast of Southern California observed by LANDSAT imagery, I, Structural characteristics, *J. Appl. Meteorol., 27*, 341-362, 1988.

Wilson, J., S. Lovejoy, and D. Schertzer, Physically based cloud modelling by scaling multiplicative cascade processes, in *Scaling, Fractals and Non-Linear Variability in Geophysics*, edited by D. Schertzer and S. Lovejoy, Kluwer, in press, 1990.

Yano, J.-I., and Takeuchi, Y., Fractal dimension analysis of horizontal cloud pattern in the intertropical convergence zone, in *Scaling, Fractals and Non-Linear Variability in Geophysics*, edited by D. Schertzer and S. Lovejoy, Kluwer, in press, 1990.

Zawadzki, I., Fractal versus correlation structure in rain, *J. Geophys. Res., 92*, 9683-9693, 1987.

S. Lovejoy, Department of Physics, McGill University, 3600 University Street, Montreal, Quebec H3A 2T8, Canada.

D. Schertzer, Météorologie Nationale, 2 Ave. Rapp, Paris 75007, France.

(Received November 14, 1988;
revised June 26, 1989;
accepted July 13, 1989.)